Journal of Cultural Heritage 50 (2021) 95–105

Contents lists available at ScienceDirect

Journal of Cultural Heritage

journal homepage: www.elsevier.com/locate/culher

Original article

Testing 1D and 2D single-sided NMR on Roman age waterlogged woods

Valeria Stagno[a,b,*], Sarah Mailhiot[c], Silvia Capuani[b,*], Giulia Galotta[d], Ville-Veikko Telkki[c]

[a] Earth Sciences Department, Sapienza University of Rome, Piazzale Aldo Moro 5, 00185 Rome, Italy
[b] National Research Council - Institute for Complex Systems (CNR-ISC) c/o Physics Department Sapienza University of Rome, Piazzale Aldo Moro 5, 00185 Rome, Italy
[c] NMR Research Unit, University of Oulu, P.O. Box 3000, 90014 Oulu, Finland
[d] Biology Laboratory, Istituto Centrale per il Restauro, Ministry of Cultural Heritage and Activities and Tourism (MIBACT), via di San Michele 25, 00153 Rome, Italy

ARTICLE INFO

Article history:
Received 16 November 2020
Accepted 4 June 2021
Available online 24 June 2021

Keywords:
Portable NMR
Chestnut
Maple
Spruce
MRI
Waterlogged archaeological woods

ABSTRACT

Waterlogged archaeological wood can provide information on past human activities and technology but its structure may be modified due to microbial deterioration. Knowing its conservation state is fundamental for its restoration. Aim of this work was to test the use of non-destructive portable NMR for the microstructural characterization and preservation state of three archaeological wood samples (Roman age, 5th century AD). 1D T_1 and T_2 relaxation time distributions, as well as 2D T_1-T_2 and D-T_2 distributions were measured by single-sided NMR and interpreted with the help of high resolution magnetic resonance imaging (MRI) and optical microscopy. Due to the complexity of the ancient wood samples, in this first study a multi-analytical approach was required. It allowed the characterization of both waterlogged softwood (spruce) and hardwood (chestnut and maple) by quantifying relaxation times and diffusion water components affected by the presence of degradation products such as fungi, paramagnetic agents, and microstructural changes. Optical microscopy was needed to investigate the sub-microscopic wood elements not resolved by MRI and validate indirect single-sided NMR investigations. Observations and results of this study will allow the improvement of single-sided NMR protocols for the analyses of archaeological wood in situ with portable NMR.

1. Introduction

Man has always used wood due to its extreme versatility and abundance [1]. To know the raw materials used in the past [2] and to record the human activity and the technology developed over the centuries [3], it is important to characterize the remains of wood saturated with water. Furthermore, it is equally important to monitor the state of preservation of waterlogged wood to study the causes of degradation and to implement new methods and materials for the consolidation and safeguarding of wooden archaeological heritage. According to the recommendation of specific European Technical Standards, in the frame of an appropriate conservation and restoration project wood characterization represents a crucial point for the knowledge of the artefact [4]. Currently, an increasing trend in choosing micro-invasive and non-invasive techniques among the different analytical methods that can be applied is observed [5–7]. However, it has to be taken into account the need of comparing different diagnostic processes, and a multi-analytical approach should be preferred to reach a more correct interpretation of the involved alteration phenomena [8,9].

In waterlogged conditions, wood suffers from both chemical-physical and biological degradation and the decay level is related to properties of wood species as well as environmental factors of the deposition site [10,11]. As regards microbial processes, tunnelling and erosion bacteria are generally the most common degraders, affecting wood in presence of oxygen and in anoxic condition, respectively [12–14]. In more oxygenated aquatic environments, wood can also be attacked by soft-rot fungi [10,15]. Erosion bacteria lead to the destruction of cell walls and pit membranes, depolymerization of hemicellulose and cellulose, while lignin is the most resistant polymer and remains better preserved even until advanced stages of decay. In heavily degraded wood, lumen and cell wall areas appear filled with decay products from the S2 and S3 cell wall layers (i.e. a mixture of bacterial slime and residual

* Corresponding authors.
E-mail addresses: valeria.stagno@uniroma1.it (V. Stagno), silvia.capuani@isc.cnr.it (S. Capuani).

https://doi.org/10.1016/j.culher.2021.06.001

lignin), while the middle lamella and S1 layer can still remain unaffected due to their higher lignin content [7,10,12]. Together with the decay products, salts and metals may be deposited within wood depending on their concentration in water and the composition of the soil in which the object is buried [16–18].

Water affects all properties relevant to the wood performance. Therefore, experimental techniques for the characterization of water inside wood are an essential part of almost all scientific research on wood materials [19]. In the last decade, the application of Nuclear Magnetic Resonance (NMR) [20] to Cultural Heritage and specifically to wood, has increased. Capitani et al. [5] suggested that a breakthrough has certainly been the development of portable single-sided (or unilateral) NMR sensors through which liquid-imbibed porous-materials of any size can be monitored in a non-destructive and non-invasive modality [21–24] thanks to the measurement of the longitudinal relaxation time (T_1), the transversal relaxation time (T_2) and the apparent diffusion coefficient of water (D).

Several works of 1D relaxation times distribution and diffusion measurements in wood by using both high and low field NMR can be found in the literature. Some authors [25–38] highlight a multimodal behaviour of NMR parameters such as relaxation times and water diffusion coefficients in both softwood and hardwood which reflects different physical and chemical environments.

The challenge of NMR parametric studies in wood is to understand how these parameters relate to the various forms of water compartmentalization in different wood parenchyma cells, vessels/tracheids and fibres to extract microstructural information from wood. Moreover, relaxation time parameters may be affected by degradation, paramagnetic agents and decay products. The limit of 1D relaxation and diffusion measurements is the difficulty correlating different environments of 1D distributions of relaxation rates and D values. On the other hand, the correlation of two NMR parameters in two-dimensional (2D) experiments is a useful tool for increasing the spectral resolution, i.e. increasing the number of water components observable.

In this regard, some papers [39–41] investigated both softwood and hardwood structure by low-field 2D T_1 and T_2 experiments at different moisture content but never at the saturation and pointed out the potential of 2D NMR to improve the peaks assignments made by 1D experiments. According to Cox et al. 2010 [39], it is possible to resolve multiple components of a softwood, spruce, during the increment of moisture content from 0% to 100% using 2D relaxation correlation spectra. The authors found out three main hydrogen reservoirs: lumen water, cell wall water and wood polymer. The cell wall reservoir is divided into two components with similar T_2 but different T_1. One component has relaxation consistent with mobile water in small voids and the other one with water bound to polymers. Bonnet et al. [40] showed the adsorption mechanisms of another softwood, Douglas fir, by 2D relaxometry at relative humidity equal to 2%, 65% and 97%. The number of 2D peaks increases when humidity increases. At 2%, there is only the peak associated with hydrogens in molecules composing wood. At 65 and 97%, there are five peaks: two free water peaks whose intensity is higher at 97%; two similar bound water components associated with earlywood and latewood of cell wall S2-layer that decrease by increasing moisture content, because the water gains mobility, and a peak with long T_1 and short T_2 belonging to wood molecules. Finally, Rostom et al. [41] is the only work that concerns the study of a hardwood sample. They analysed the T_1-T_2 behaviour of modern and ancient oak at 65% of relative humidity and measured four main 2D peaks: liquid water in lumen, two reservoirs of bound water in cell wall and H atoms of wood polymers. Furthermore, Hiltunen et al. [42] showed that T_1-T_2 experiments provide detailed information about the changes in the microstructure of wood due to fungal decomposition. On the other hand, due to the high potential of NMR diffusion in the porous media studies [43,44], it would be very useful to associate the respective relaxation times to different diffusive compartments.

2. Research aim

This paper aims to test the feasibility of low-field unilateral NMR to investigate archaeological waterlogged wood samples by both 2D T_1-T_2 and D-T_2 correlation spectroscopy and by 1D relaxometry. To the best of our knowledge, this is the first single-sided NMR study of waterlogged wood and the first D-T_2 NMR study of wood. Here, the combined approach of 1D and 2D NMR is exploited to provide a non-destructive characterization of water compartments and highlight the presence of decay processes in three different Roman age archaeological wood samples of softwood and hardwood. Importantly, for this preliminary approach, high-field NMR images (MRI) and optical microscope images were acquired to validate single-sided indirect NMR investigations. Indeed, in a first phase, the indirect structural information provided by NMR must be validated by complementary different techniques already accredited for the study of wood structures, such as optical microscopy.

3. Experimental procedures

3.1. Materials

Three archaeological waterlogged wood samples with a diameter of 8 mm and height of 15 mm were studied in their original state and size during low-field and high-field NMR experiments, while they were cut for optical microscopy investigation. The species of wood have been identified in a restoration study by *Istituto Centrale per il Restauro* [45] as common spruce (*Picea abies* Karst.), sweet chestnut (*Castanea sativa* Mill.) and maple (*Acer* L.) [46–48]. Each sample was detached from three different poles of a wooden pier dated to the Roman age (specifically 5th century AD) and recovered in 2018 in the archaeological excavation area of the ancient harbor of Neapolis (Naples, Italy) [49,50]. The wood samples were waterlogged until their discovery in 2018 and then stored in distilled water at 4°C. Moreover, an imbibed modern wood sample of maple (*Acer* L.) was used for the optical imaging comparison with the archaeological maple.

3.2. Methods

3.2.1. 2D correlation spectroscopy

The pulse sequences for the T_1-T_2 and D-T_2 correlation experiments used in this work are shown in Fig. 1. Typically, for low-field acquisitions the T_1-T_2 correlation spectroscopy is performed using a Saturation-Recovery sequence followed by a Carr-Purcell-Meiboom-Gill (SR-CPMG) sequence [39]. In the case of D-T_2 experiments, diffusion is encoded with a Static-Gradient Stimulated-Echo (SGSTE) sequence because the magnetic field gradient of the single-sided instrument cannot be varied [51–53]. By varying the delay δ time, the sensitivity to diffusion can be varied systematically [51]. The diffusion encoding is followed by the CPMG sequence which both encodes T_2 relaxation and acquires the signal.

To extract T_1-T_2 and D-T_2 distributions, a 2D Inverse Laplace Transform (ILT) algorithm [51,54–63] is used. This algorithm is fast and efficient and provides 2D correlation spectra of the system but also has a few limitations [63]. The ILT method is affected by the presence of noise that can produce artefacts [52,63]. There exist infinite number solutions consistent with the data and therefore regulators are necessary [52,63]. Furthermore, the method can split up a broad signal into set of narrow peaks [63].

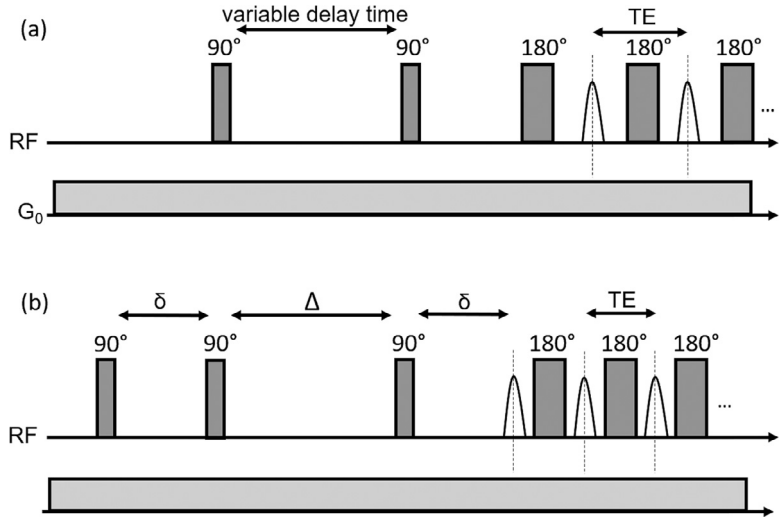

Fig. 1. (a) SR-CPMG sequence diagram used for T_1-T_2 experiment and (b) SGSTE-CPMG sequence diagram used for D-T_2 experiment.

3.2.2. Low-field single-sided acquisitions

For the low-field acquisitions, the water soaked woods were placed on the bottom of an empty glass beaker sealed with Parafilm in order to prevent dehydration. The beaker was used in order to cover all the sensitive area of the radiofrequency coil. The sample was positioned in the center of the sensitive area and its volume was scanned by lift the positioning. Specifically, measurements were taken at 5 mm from the sample surface. Each sample was placed with its longitudinal direction (i.e. the direction parallel to the main axis of wood cells, that is parallel to the long axis of the sample) parallel to the static magnetic field B_0 direction and perpendicular to the field gradient direction. Therefore, diffusion was measured along the transverse (radial or tangential) direction of wood samples. Low-field single-sided Magritek PM25 profile NMR-MOUSE with the ^{1}H resonance frequency of 13 MHz, maximum depth of 25 mm, resolution of the 1D profile of the sample equal to 100 μm and constant magnetic field gradient of 8 T m^{-1} was used to perform longitudinal (T_1) and transversal (T_2) relaxation experiments, as well as T_1-T_2, and D-T_2 correlation spectra acquisitions using Prospa V3.39 software.

For obtaining T_1 relaxation times, a Saturation-Recovery (SR) sequence was used with repetition time (TR) of 4000 ms, number of scans (NS) = 128, minimum/maximum variable delay time =1/2000 ms, and 32 exponentially increasing recovery time values. The experiment time was 4.5 h.

A Carr-Purcell-Meiboom-Gill (CPMG) sequence with echo time (TE, the time between 180° pulses) of 150 μs, TR=3500 ms, 1000 echoes, and NS=128 was used to evaluate T_2 relaxation times. The experiment time was 7.5 min.

To acquire T_1-T_2 2D correlation spectra, a SR-CPMG pulse sequence was used. The two-dimensional acquisition modality was obtained using TR=4000 ms, NS=128, 32 exponentially increasing variable delay time, minimum/maximum variable delay time of 1/2000 ms, 600 echoes, and TE=150 μs. The experiment time was 4.5 h.

To obtain D-T_2 2D correlation spectra, a Static-Gradient Stimulated-Echo sequence (SGSTE) followed by a CPMG sequence was used with TR=3500 ms, NS=128, 32 gradient length increments with minimum/maximum gradient length δ=0.2/1 ms, TE=150 μs, 600 echoes, constant gradient strength (g) equal to 8 T m^{-1}, and diffusion time Δ=1 ms. Due to the T_1 decay that would occur during Δ in a PGSTE experiment or the T_2 decay that would occur during Δ in a PGSE experiment, for these first acquisitions we used a small Δ to be definitely in the condition $\Delta < T_1, T_2$. The total experiment time was 3.7 h.

In both T_1-T_2 and D-T_2, the experiment time is around 4 h and the CPMG sequence can lead to heating of the sample. Therefore, in order to mitigate the effect of heating the sample was kept in a sealed glass beaker that worked as a humidity chamber for the duration of measurements.

All data were processed by using Inverse Laplace Transform (ILT) [64] in MATLAB (MATLAB R2019a) to achieve T_1 and T_2 fits and to obtain T_1-T_2 and D-T_2 maps.

3.2.3. High field MRI

To perform high field NMR imaging experiments, the wood specimens were inserted in a 10 mm NMR glass tube with distilled water. The tube was sealed with Parafilm in order to prevent water evaporation. The longitudinal direction of the sample was parallel to the direction of the static magnetic field B_0. A Bruker Avance III 300 MHz spectrometer equipped with a Micro 2.5 imaging probe, 10 mm radio frequency insert and a maximum gradient strength of 0.95 T m^{-1} was used. ParaVision® 5.1 software was employed for data acquisition and image processing. Transversal-view images i.e. perpendicular to the main axis of cells were selected. For each wood specimen, a Multi-Slice Multi-Echo (MSME) sequence with TE=15.6 ms, number of echoes = 1, TR=0.5 s and 8 s, NS=16, field of view (FOV)=12×12 mm^2, matrix (MTX)=512×512, slice thickness (STK)=0.5 mm, in plane resolution (R)=23×23 μm^2 was run. The experiment time for each image was 1 h when TR = 0.5 s and 18 h when TR = 8 s. The NMR and MRI data used in this work is publicly available [65].

3.2.4. Optical microscopy

To carry out optical microscopy investigations thin xylem sections (10-20 µm thick) on the transversal anatomical planes (i.e. perpendicular to the longitudinal axis of the grain) for each sample and on the longitudinal plane only for spruce wood were obtained by cutting frozen small cubes (about 5 mm side) either by hand with a razor blade or by cryo-microtome (Cryostat CM 1900, Leica). Sections were mounted on slides with a drop of glycerol. No embedding medium was applied. Images were obtained by using an Axio Imager.M2, Zeiss optical microscope equipped with digital camera both in normal and polarized light and processed by Zen 2.3 Pro software in a range of magnification between 50 and 200 times.

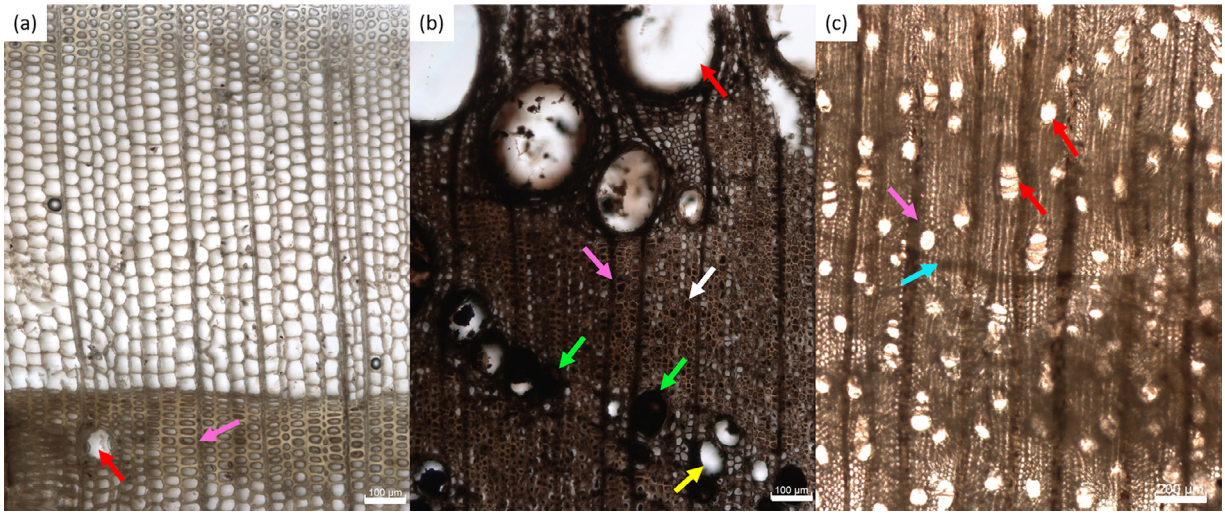

Fig. 2. Optical microscopy images of (a) spruce wood characterized by resin ducts (red arrow) bordered by thick-walled epithelial cells and uniseriate parenchyma rays (pink arrow); (b) chestnut wood with large earlywood vessels (red arrow) and small latewood vessels (yellow arrow) arranged in dendritic pattern, presence of inclusions (green arrows) filling cell lumina of vessels, axial parenchyma cells and fibres, inclusions in cell cavities (white arrow), and uniseriate parenchyma rays, which are rarely biseriate (pink arrow); (c) maple wood with numerous small to medium vessels (red arrows), solitary or in radial multiples of 2-4 elements, growth ring boundaries distinct by radially flatted fibres (light blue arrow), and multiseriate rays (pink arrow). Bar scale: 100 µm in (a) and (b), and 200 µm in (c).

4. Results

4.1. Optical microscope images: wood anatomy

In Fig. 2a spruce wood shows a gradual transition from earlywood to latewood. It has resin ducts, indicated by a red arrow, bordered by thick-walled epithelial cells and uniseriate rays, indicated by a pink arrow.

Fig. 2b shows the chestnut microstructure with vessels larger than 200 µm in the earlywood, indicated by a red arrow and smaller vessels in the latewood indicated by a yellow arrow. Latewood vessels are arranged in dendritic pattern. The white arrow highlights cell lumen inclusions. In addition, this wood has uniseriate, rarely biseriate, parenchyma rays which is indicated by a pink arrow. The green arrows indicate obstructed vessels.

In Fig. 2c maple microstructure is displayed. This sample has numerous (20-40 up to 100 vessels per square millimeter) small to medium vessels (50-100 µm, red arrows) solitary or in radial multiples of 2-4 elements. The growth ring boundaries are distinct by radially flattened fibres indicated by the light blue arrow and the rays are multiseriate, indicated by the pink arrow.

4.1.1. Evaluation of decay

As already observable in Fig. 2a, an incipient microbial decay of spruce wood, referred both to cellulolytic bacteria and fungi is better visible in Fig. 3a–c. A layer of dark-coloured substance, with a grainy appearance, formed by erosion residual wood products adhered with bacterial extracellular mucilage can be observed facing the cell lumen mainly in the secondary wall of latewood tracheids (Fig. 3a, red arrow). Polarized light microscopy highlights the well preserved structure of compound middle lamellae and secondary cell walls, appearing bright due to the birefringent nature of the cellulose. Conversely, the inner part of secondary walls is converted into an amorphous substance, which extinguishes the polarized light and appears darker (Fig. 3b). A fungal incipient attack is testified by the presence of hyphae passing through the cells (Fig. 3a and c, white arrows) and typical soft rot erosion tunnels, visible in longitudinal section (Fig. 3c, pink arrows). As the samples were kept in water without preservatives after the archaeological excavation, these results may attest resumption of a post-excavation fungal colonization.

In Figs. 2b and 3d inclusions are indicated by green arrows and are observed in both earlywood and latewood vessels and in some cases small vessels are completely obstructed. We may suppose these black-coloured inclusions are iron-tannin precipitates. For tannin-rich species, such as chestnut and oak, the presence of iron-tannin complexes in waterlogged archaeological finds is well known. It is linked to the chelating capability of polyphenols of forming stable complexes with iron, not only coming from metallic parts of the artefact but also simply presents in the burying sediments [16,18]. A rather advanced state of degradation, ascribable mainly to erosion bacteria, can be observed with a generalized detachment and loss of fibres secondary walls (Fig. 3d), although the lignin-cellulose structure of compound middle lamella is still well preserved as shown through polarized microscopy (Fig. 3e).

Differently by the previous woods, in maple images (Fig. 3f and g) no complete cell wall detachment can be clearly distinguished. Nevertheless, the weak and spongy consistence of wood accounts for a significant decay. Thinning of fibres cell wall can be observed at normal (Fig. 3f) and polarized light (Fig. 3g). A certain amount of cellulose birefringence went definitely lost, as it can be clearly observed at polarized microscopy by comparison with a recent wood reference (Fig. 3h). Also in this case the presence of spores and residues of fungal hyphae in the cellular lumens should be noted (Fig. 3f, white arrow).

4.2. MR images

Transversal-view T_1 and T_2-weighted images with TR=0.5 s are shown in the upper row of Fig. 4 while those acquired with TR=8 s are displayed in the lower row. Images of spruce are displayed in Fig. 4a and d, chestnut in 4b and e, and maple in 4c and f. Due to the relatively long echo time in the MRI (15.6 ms), only free water is visible in the images. TR changes the image contrast: distilled water with long T_1 around the samples is highlighted in the long TR images, while the water signal from the wood samples is highlighted in the short TR images. The cross-sections of tracheids and vessels are visible in the MR images. MR images in Fig. 4 allow observing homoxylous structure (Fig. 4a and d)

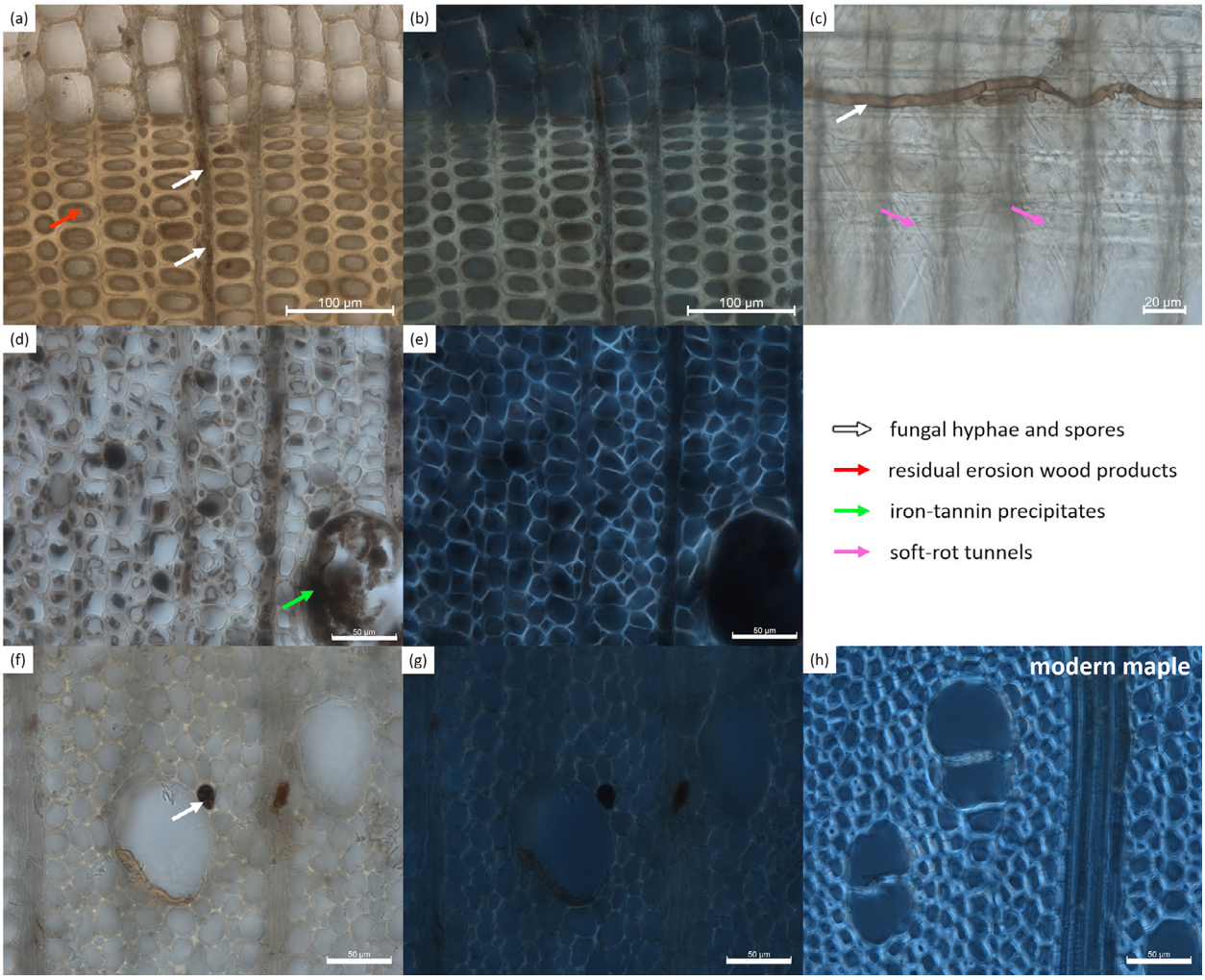

Fig. 3. Optical microscopy images showing biological decay details. Spruce wood transversal section at normal light (a) and polarized light (b) with only better preserved layers of secondary walls and middle lamellae appearing bright. In (c) spruce radial section at normal light. Chestnut transversal section at normal light in (d) with detachment and loss of fibres secondary walls and at polarized light in (e) with only middle lamellae well preserved. Ancient maple transversal section at normal light (f) showing a general thinning of cell walls and at polarized light in (g) cellulose birefringence reduction compared to the modern sample in (h). Bar scale: 100 μm in (a) and (b); 20 μm in (c); 50 μm in (d-h).

[66] with resin ducts (indicated by yellow arrow), uniseriate rays (red arrow) and well distinguishable annual rings (pink arrow) in the softwood spruce. Each annual ring shows two areas with different image contrast in agreement with the literature [29,30,37,67]. The brighter area is representative of earlywood (green arrow) characterized by pores (lumens of tracheids) with a bigger cavity and thinner walls compared to those of latewood zone. The darker and less extensive area is the latewood (blue arrow) characterized by smaller pores and thicker walls [68]. In Fig. 4a and d, several black spots and artefacts are visible. There is a diffuse presence of black spots (artefacts) on a grey background (representative of earlywood) with darker grey zones (representative of latewood) and few brighter areas corresponding to more hydrated structures characterized by a longer T_2. In comparison with the optical images (Figs. 2a and 3a, c) we can suppose that black spots and artefacts are due to a dramatic drop in signal caused by field inhomogeneities generated by the presence of paramagnetic substances which are strong relaxants for the spin system. Another interpretation for black spots is that they may be due to lack of signal produced by solid residues. We may associate these black spots to erosion residual wood products and the presence of fungi.

Images in Fig. 4b and e show the heteroxylous structure in the hardwood chestnut [69]. Chestnut structure is seen in the MR images with a very dark background in latewood as indicated by the blue arrow and large cross sections of vessels as white voxels (orange arrow) in the earlywood zone (green arrow). As in Fig. 4e the image is T_2-weighted, the black voxels indicate low T_2 values, less than 15.6 ms. This may be due to a degradation process that produced an accumulation of paramagnetic agents in the parenchyma, fibres, latewood vessels and partially in earlywood vessels. These paramagnetic agents may correspond to iron-tannin precipitates whose presence was previously hypothesized by the optical investigation (Figs. 2b and 3d, e). On the other hand, the white voxels indicate higher T_2 values, due to bulk-like water in large vessels cross-sections. Therefore, the presence of a ring-porous composed by huge vessels in the earlywood area and few smaller vessels in latewood is easily visible also by MRI.

A different microstructure can be observed in Fig. 4c and f. The hardwood maple appears with vessels, indicated by an orange arrow, in diffuse-porous configuration. The vessels cross–section have roughly the same size. The surrounding wood is composed by fibres indicated by light blue arrow. In addition, rather large rays, indicated by the red arrow, and annual ring limit, indicated by the pink arrow, are well discernible. The greater overall signal intensity may imply that maple contain less paramagnetic impurities.

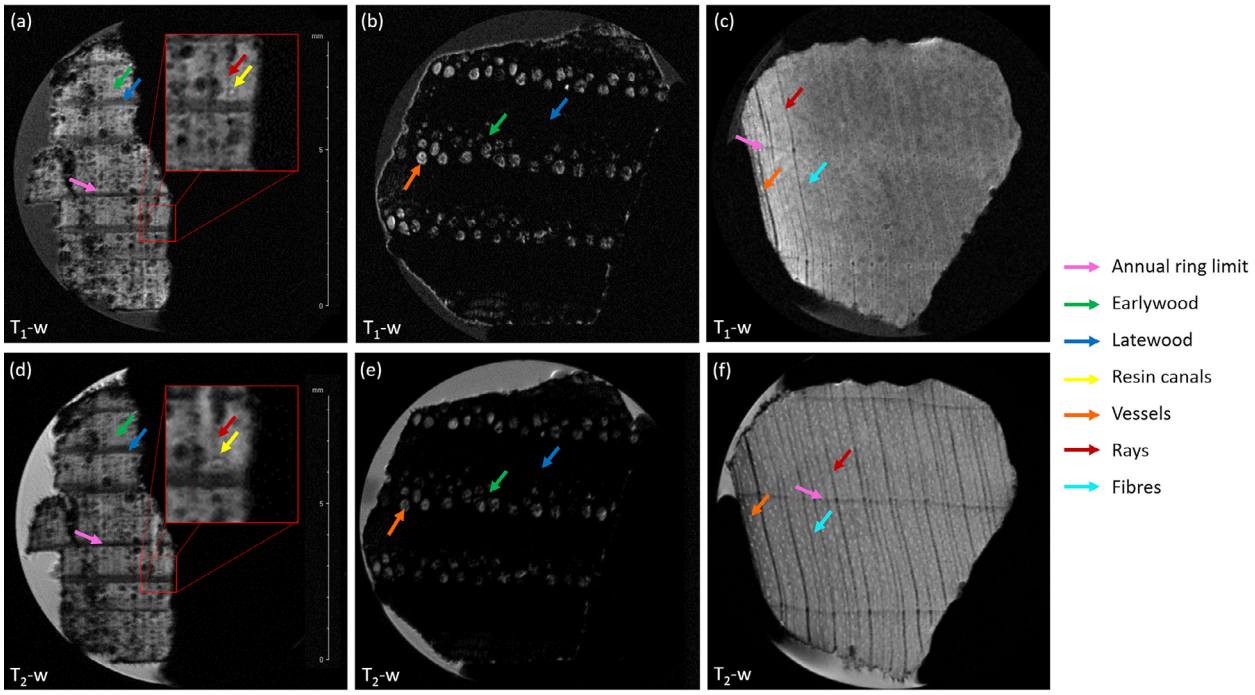

Fig. 4. Transversal view T_1 and T_2-weighted images acquired at TR=500 ms and TR=8000 ms for common spruce (a, d), sweet chestnut (b, e) and maple (c, f). Several diagnostic characters are highlighted by arrows. The black spots and artefacts are due to paramagnetic impurities and fungi. For each image, the slice thickness = 0.5 mm and in plane resolution = 23x23 μm^2.

4.3. 1D relaxometry and 2D T1-T2 and D-T2 experiments

1D T_1 and T_2 relaxation time distributions of the wood samples are shown in Fig. 5a and b, respectively. Because of the less heterogeneous structure of softwood compared to hardwood, the spruce sample shows only one T_1 component and two T_2 components. On the other hand, chestnut is characterized by three components in both T_1 and T_2 distributions and maple shows two components in both distributions.

2D T_1-T_2 and D-T_2 correlation maps are displayed in Figs. 6 and 7, respectively. In the maps the colour bar from bottom to top represents the increasing intensity or abundance of the correlated spins population. In Fig. 6 the dashed red line indicates T_1=T_2. In Fig. 7 the red dashed line indicates the free water diffusion coefficient D=2.2×10^{-9} m^2 s^{-1}.

The T_1-T_2 correlation spectra of spruce wood in Fig. 6a includes four peaks labelled A, B, C and D, instead of two peaks found from the T_2 distribution or one found from the T_1 distribution. A T_1/T_2 ratio of about 6 is the same for peaks A, B and C but it is bit higher, about 10, for D. Overall, the T_1/T_2 ratios are higher than those observed for the same wood species at the low-field of 20 MHz by Cox et al. 2010 [39] that are around 2 for bulk water. This is possibly due to the shortened observed T_2 values in the single-sided NMR experiments caused by the strong, constant gradient (see Discussion). For chestnut sample (Fig. 6b), the four main T_1-T_2 correlation peaks or peak groups, labelled by A, B, C and D have a wider spread of relaxation time values and highlight a more complex water compartmentalization. The T_1/T_2 ratio of peaks group A is very high, around 20, due to the high relative shortening effect of the gradient on long T_2 values. Peaks B, C and D are characterized by T_1/T_2 ratios from 1 to 2. Maple shows three different T_1-T_2 correlation peaks (Fig. 6c), instead of two peaks visible in the T_1 and T_2 distribution. The T_1/T_2 ratio of about 6 is quite similar to spruce wood. For all the samples, the number of T_1 and T_2 components observed in the 2D experiments is increased if compared to the 1D experiments. It might be that the resolution in the 2D T_1-T_2 is higher than in the 1D T_1 and T_2 experiments; on the other hand, some splitting may also be a consequence of so-called pearling artefact typical for Laplace inversion [63].

In Fig. 7, D-T_2 maps are displayed for each wood sample. Spruce map shows two clearly distinguished peaks or peak groups, A and B. Chestnut is characterized by four peaks or peak groups A, B, C and D. Finally, maple shows two D-T_2 peaks, peak A with the diffusion coefficient close to that of the free water and peak B with a lower D value. There are additional small amplitude peaks visible, which are artefacts arising from the experimental noise.

5. Discussion

Single-sided NMR is mobile and suitable for the in-situ non-destructive characterization of cultural heritage [3,5,70]. However, unilateral NMR is intrinsically limited since it provides an indirect measure of medium microstructure and relies on inferences from models and estimation of T_1, T_2 and D parameters. Therefore, it is necessary to validate the information obtained by portable NMR through complementary investigations. To test the potential of single-sided NMR for the study of the preservation state of archaeological wood, results obtained by low-field portable NMR, high-field high resolution MRI and optical microscope images were compared for each of the three waterlogged samples investigated. Optical microscopy can provide images with a resolution of few micrometers or less, but it requires a destructive mechanical sectioning. On the other hand, MRI can be non-destructive and provides volumetric information [67] but its current resolution (linear resolution of tens of micrometers) is still insufficient to detect all microscopic features of woods. However, MRI can highlight the presence of decay and can help in the low-field results interpretation but it is important to underline that optical microscopy can identify fungi and bacteria, which result in non-specific structural alterations in MR images.

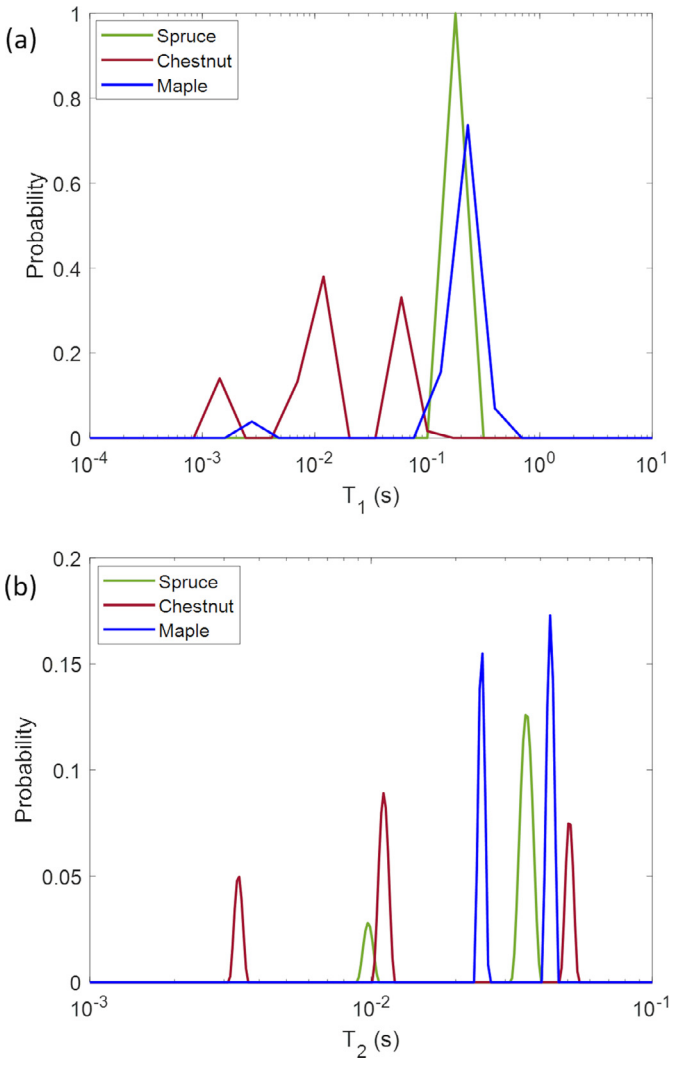

Fig. 5. 1D T_1 (a) and T_2 (b) distributions for the three wood samples studied.

When interpreting the low-field T_2 results, it is important to note that the observed apparent T_2 values are heavily affected by the molecular diffusion in the presence of the strong (8 T m^{-1}), constant magnetic field gradient of the single-sided instrument [71,72]. The echo amplitude in the CPMG experiment is [73,74]:

$$E(t) = E_0 \exp\left[-\left(\frac{1}{T_2} + \frac{\gamma^2 g^2 \tau^2 D}{3}\right)t\right] \quad (1)$$

where E_0 is the initial echo amplitude, γ is the nuclear gyromagnetic ratio, g is the strength of a constant magnetic field gradient and τ is the delay time between the first 90° and 180° pulses. Therefore, the observed apparent T_2 value, T_{2app}, is much shorter than true T_2:

$$\frac{1}{T_{2app}} = \frac{1}{T_2} + \frac{\gamma^2 g^2 \tau^2 D}{3} \quad (2)$$

In the experiments described in this paper, τ was 75 μs (echo time 150 μs) and g was 8 T m^{-1}. If $D = 2.2\times10^{-9}$ m^2 s^{-1}, the maximum observable value of T_{2app} is 53 ms (assuming that $T_2^{-1} \approx 0$). If the true T_2 is equal to 1, 10, 50 or 100 ms, the observed T_{2app} is 0.98, 8.4, 26 or 35 ms, respectively. On the other hand, D observed in the transverse direction of wood is typically 1×10^{-9} m^2 s^{-1} or less [75,76] due to the restricted diffusion, corresponding to the maximum T_{2app} of 116 ms. If $D = 1\times10^{-9}$ m^2 s^{-1} and if

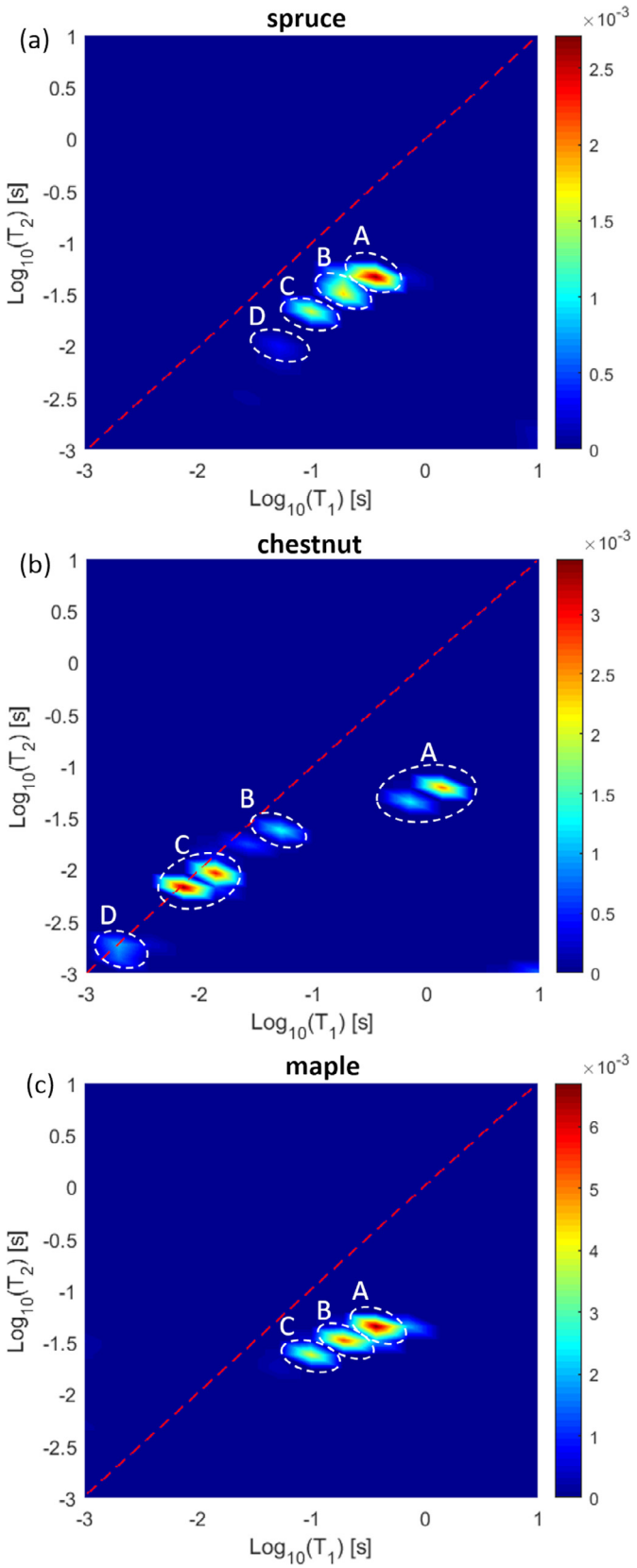

Fig. 6. 2D T_1-T_2 maps of (a) common spruce, (b) sweet chestnut and (c) maple. On the right the colour bar represents from bottom to top the increasing intensity of the peaks. The red dashed line indicates T_1=T_2.

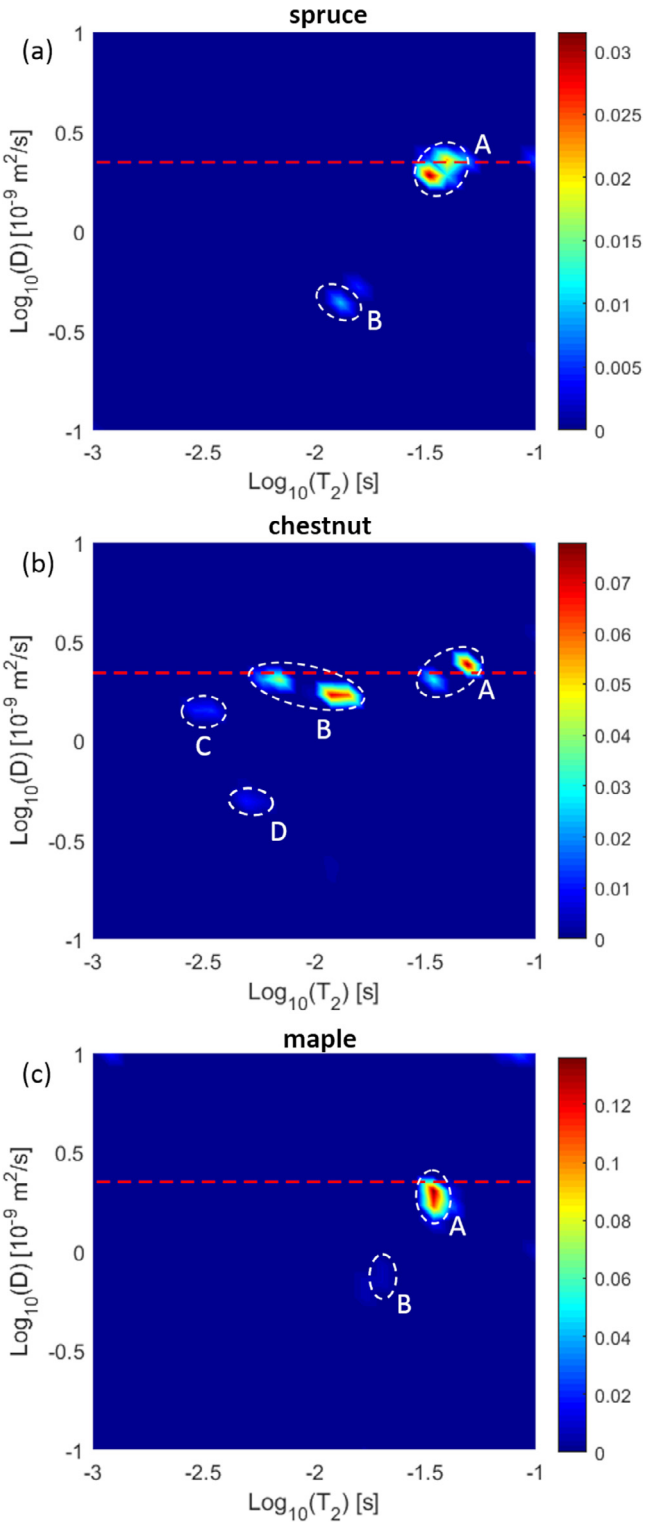

Fig. 7. 2D D-T_2 maps of (a) common spruce, (b) sweet chestnut and (c) maple. On the right the colour bar represents from bottom to top the increasing intensity of the peaks. The red dashed line indicates the bulk water D=2.2x10^{-9} m^2 s^{-1}.

the true T_2 is 1, 10, 50 or 100 ms, the observed T_{2app} is 0.99, 9.2, 35 or 54 ms, respectively. The shortening effect is relatively more significant for longer T_2 values.

The component of bound water, which is typically around T_2 = 1 ms [34,38] is absent in the T_2 distribution due to the degradation of the cell walls discussed in section 4.1.2. This may be a consequence of both the decreased amount of bound water and the accelerated exchange between bound and free water due to the cell wall degradation [42]. Furthermore, in the D-T_2 experiment, the diffusion delay Δ was only 1 ms. The effects of restricted diffusion could be enhanced by using longer Δ, potentially providing additional contrasts on the structural details [75,76].

5.1. Common spruce

In the MR images (Fig. 4a and d) the many dark spots represent places where signal is not detected, either due to a lack of signal or a very short T_2. A short T_2 or a lack of signal can be associated with the presence of paramagnetic impurities or solid residues that may correspond to erosion products and fungi (see Fig. 3a–c).

Typically, water in softwood tracheids has T_2 between 9-400 ms and a T_1 that is one order of magnitude higher than T_2 [31,35]. In this sample, while the peak in Fig. 5a with T_1=180 ± 70 ms is similar to that measured with a standard spectrometer [34] and can be interpreted as bulk water in structures with a diameter around 20-40 μm [67], the observed apparent T_2 values were significantly shortened due to the gradient. We hypothesize that the longer T_2 component (T_2=36 ± 3 ms) comes from earlywood tracheids, where the lumens are much larger than in latewood (see the optical microscopy images in Fig. 2a). This is in agreement with previous studies in which T_2 values between 30-400 ms have been associated with larger lumens in earlywood or resin canals [31,35,70] and with the MR images, where the signal is predominantly originating from bulk water in earlywood tracheid lumens (green arrows in Fig. 4a and d). Conversely, the darker contrast in the MR images corresponds to areas with shorter T_2 [77]. Some authors [31,35,70] interpreted components of T_2 between 9-80 ms as smaller lumens in latewood and ray cells (see Fig. 2a). In this work we detected a T_2 of 10.0 ± 0.3 ms that can be associated with water in rays (pink arrow in Fig. 2a and red arrows in Fig. 4a and d) and latewood area (blue arrows in Fig. 4a and d), with the presence of decay impurities as observed in both MR images (Fig. 4a and d) and optical images (Fig. 3a, red arrow). The peak area associated to earlywood in Fig. 5b is higher than that of the latewood reflecting the smaller lumens volume of latewood as compared to earlywood (see MR images in Fig. 4a and d and optical microscopy image in Fig. 2a).

The 2D T_1-T_2 correlation map (Fig. 6a) implies the existence of four distinct populations of spins A, B, C and D, although some peak splitting might also be a consequence of the pearling artefact. Thanks to the higher resolution of 2D experiments compared to 1D counterparts, it is possible to discriminate similar values of T_1 that in 1D measurements appeared as a single peak. The most intense peaks A-C with longer T_1 and T_2 represent free water in earlywood (green arrows in Figs. 4a and 4d) specifically with water in bigger lumens (see Fig. 2a) which is in agreement with previous works [29-31, 35]. Peak D is characterized by shorter T_1 and T_2 and it can be associated with water in latewood tracheids and rays (Fig. 2a, pink arrow) [31, 35]. Again, the greater intensity of peaks A-C as compared to peak D reflects the larger earlywood area and lumen volume as compared to latewood in agreement with MR images (see Fig. 4a and d), optical microscopy (Fig. 2a) and 1D T_2 relaxation (Fig. 5b).

The D-T_2 map (Fig. 7a) includes peak group A with D = (1.9-2.3)x10^{-9} m^2 s^{-1} and T_2 = 33-40 ms. The diffusion coefficient is close to that of the free water (red dashed line in Fig. 7a) and together with the quite similar T_2 value can be associated with two water compartments in the earlywood area, in agreement with the results of T_1-T_2 map (see Fig. 6a). The second peak B is characterized by a lower D = 0.4×10^{-9} m^2 s^{-1} and T_2 = 13 ms that can be associated with the restricted water diffusion in rays (pink arrow in Fig. 2a) and in latewood tracheids (blue arrows in Fig. 4a and d)

that are obstructed by residual erosion wood products and fungal hyphae (see red and white arrows in Fig. 3a and c). Peak group A is more intense than peak B, which confirms the greater area and lumen volume of earlywood compared to latewood in agreement with T_1-T_2 map and T_2 distribution.

5.2. Sweet chestnut

This wood shows much shorter T_1 values (Fig. 5a) than that expected of the free water environments shown in MR images (Fig. 4b and e) and optical microscopy image (Fig. 2b). Both in MR and optical images, the whole sample has a dark contrast due to very low NMR signal and low light transmission, respectively. This specific contrast is supposed to be due to the presence of iron-tannin precipitates observed by light microscopy of Fig. 3d and e and typical of tannin-rich species as chestnut. Nevertheless, there are also water molecules in the huge vessels, which are larger than 200 µm (orange arrows in Fig. 4b and e, red arrow in Fig. 2b), that should have relaxation times comparable to free water. The low T_1 values shown in Fig. 5a (red curve) seems to confirm the high concentration of paramagnetic impurities (i.e. iron-tannin complexes) and erosion products (green arrows in Figs. 2b and 3d). The intensities of intermediate T_1 =12 ± 5 ms and T_2 =11 ± 1 ms peaks are the highest. Since the T_1 values are affected by the impurities, we can assign only the T_2 components to the anatomical structures of this wood. The rightmost peak in Fig. 5b is around 50 ± 2 ms and can be related to bulk water in vessels [26,28,36]. The shorter T_2 values around 11 ± 1 and 3.4 ± 0.1 ms could belong to bulk water in latewood vessels and in rays (pink arrow Fig. 2b), parenchyma and degraded cell walls (white arrow Figs. 2b and 3d and e), respectively [26,28,36].

The T_1-T_2 map shows four peaks or peak groups, A, B, C and D (Fig. 6b). Peaks A have the longest T_1 and the highest T_1/T_2 ratio due to the shortening effect of the gradient. Peaks A most likely arise from free water on the surface of the sample due to its long T_1 relaxation time (about 1 s). Peaks B and C belong to water in earlywood and latewood vessels, respectively (see Fig. 4b and e, orange arrows, and Fig. 2b, red and yellow arrows). Their T_1/T_2 ratio is ~ 1.5. Peak D is linked to bound water in parenchyma or rays (pink arrow Fig. 2b) and in degraded cell walls (white arrow Fig. 2b), respectively, with very low mobility. Peaks group C has the most intense signal suggesting a large amount of bulk water in the large vessels of chestnut. The intensity of peak B, which is also associated with vessels, may be underestimated because of the presence of impurities stored in the vessels lumen (see Figs. 2b and 3d) caused by the deterioration process.

The D-T_2 map of the chestnut shows three main populations (Fig. 7b). Peaks group A indicates a population of spins with D = (2.0-2.4)x10^{-9} m^2 s^{-1} and T_2 = 35-49 ms. These values are associated to bulk water in the large vessels of earlywood, in agreement with the T_1-T_2 results. Peaks group B has D = (1.7-2.0)x10^{-9} m^2 s^{-1} and T_2 = 7-12 ms that can be interpreted as a more restricted water in the latewood vessels. Peaks C and D have D around (0.6-1.9)x10^{-9} m^2 s^{-1} and T_2 of 3-5 ms. This T_2 is similar to that of peak D measured in T_1-T_2 map and can be attributed to water molecules in parenchyma, rays and degraded cell walls. The intensity of the peaks suggests a higher amount of water in vessels and a lower amount in rays and parenchyma, which agrees with the MRI and T_1-T_2 experiments.

5.3. Maple

As shown in the MR images (Fig. 4c and f) and optical microscopy image (Fig. 2c) this wood has a quite homogeneous diffuse-porous ring structure made of vessels and fibres that have a T_1 of 220 ± 90 ms (Fig. 5a). Moreover, in Fig. 5b the two different T_2 values of 43 ± 2 ms and 25 ± 1 ms reflect the bulk water in maple vessels with the size of 50-100 µm, and in fibres (light blue arrow in Fig. 4c and f), respectively. The minor T_1 peak around 3 ms might be associated with degraded cell walls, but it might also be an artefact, as corresponding peak was not observed in the T_1-T_2 experiment. The peaks in Fig. 5b have similar intensities to each other because there is a similar amount of water in vessels and fibres in this wood.

The T_1-T_2 map shows three different populations A, B and C (Fig. 6c). Peaks A and B are associated with water inside two clusters of vessels with very similar T_1 and T_2 and are also the most intense according to 1D results (Fig. 5b). Peak C represents the fibres that, conversely to the other analysed woods, here have water content comparable to vessels, as shown by the similar contrast in Fig. 4c and f. This is corroborated by the light microscopy results in which the fibres cell walls are thinned (Figs. 3f and 3g).

Two peaks, called A and B, were observed in the D-T_2 map (Fig. 7c) of the maple wood. The diffusion coefficient of peak A is 2.0×10^{-9} m^2 s^{-1} and its T_2 around 35 ms. These values indicate water in vessels. Peak B has lower D value of 0.63×10^{-9} m^2 s^{-1} and T_2 of about 35 ms, and it can be likely associated to water in fibres.

5.4. Inferred wood microstructures by single-sided NMR parameters T_1, T_2, D

Regarding the wood microstructures, single-sided investigation suggests that spruce has two main clusters of pores, earlywood and latewood tracheids with the former one more abundant the latter. Earlywood pores are characterized by higher values of T_2 and D that means they are larger than latewood pores. Moreover, well preserved structure of middle lamellae and secondary cell walls was observed while the inner part of secondary walls is converted into amorphous substance. This wood shows artefacts which might be associated to erosion residual wood products together with fungal hyphae and soft rot fungi. The decay distribution appears mostly along the rays, in latewood tracheids and on the edge of the sample. Sweet chestnut has the largest vessels in which water diffusion is free, but some of them are obstructed by impurities which might be iron-tannin precipitates. This yields to a strong dependence of the longitudinal relaxation time (T_1) from the paramagnetic iron impurities and produces an overestimation of the water abundance in the cell walls. Despite the large degree of decay operated by erosion bacteria, the lignin-cellulose structure of compound middle lamella is still well preserved. So, chestnut is mainly composed of two clusters of vessels (i.e. in the earlywood and latewood), parenchyma and rays. Maple seems to be the only wood with no visible cell wall detachment but spores and residues of fungal hyphae are observed in the cellular lumens. Maple wood shows two types of structures, vessels and fibres, with a similar water behaviour and content due to the fibres cell walls thinning.

6. Conclusion

This work suggests a preliminary protocol to test the feasibility of single-sided low-field NMR in a first characterization of archaeological waterlogged wood. A portable instrument allows to perform in situ analysis and to study samples of any size. Due to the complexity and decay of wooden remains, complementary information provided by high field MRI and optical microscopy images, which require a destructive sampling, was used for the interpretation and validation of 1D relaxometry, 2D T_1-T_2 and D-T_2 results obtained by single-sided NMR. We suggest that the combination of 1D and 2D acquisitions is useful to reveal water compartmentalization from which possible microstructural configura-

tions of wood can be extrapolated. In this work, as a consequence of the decay process, the archaeological wood samples are devoid of bound water characterized by T_2 around 1 ms which instead is found in studies carried out on contemporary wood [34,38]. This suggests the ability of single-sided NMR of detecting cell wall decay. Conversely, due to the current limited resolution of MRI (about $10\times10\mu m^2$ in plane resolution), is not possible to directly observe cell wall decay. Moreover, single-sided NMR can be useful to detect paramagnetic impurities in wood, such as heavy metals complexes, iron, and salts. This feature of single-sided NMR is also supported by MRI, which shows black spots in images. This information is complementary to that provided by light microscopy investigation. Overall, this work suggests that single-sided NMR may be a useful in situ investigation tool to a preliminary and complementary investigation of archaeological wood totally soaked in water.

Acknowledgments

The authors would like to thank funding of Lazio Region (Italy) under Torno Subito 2018 program of the Department of Education, Research, School, University and the Regional Body for the Right to Study and Knowledge (DiSCo). V.-V.T. thanks the European Research Council (ERC) under Horizon 2020 (H2020/2018-2022/ERC) [grant number 772110], Academy of Finland [grant numbers 289649, 294027 and 319216], the Kvantum institute (University of Oulu) and the CA15209 COST action (EURELAX) for financial support. S.M. thanks the Academy of Finland [grant number 321701].

The Laplace inversion program used in this work was provided by the group of late Prof. P. Callaghan.

References

[1] W.H. Schoch, G. Bigga, U. Böhner, P. Richter, T. Terberger, New insights on the wooden weapons from the Paleolithic site of Schöningen, J. Hum. Evol. 89 (2015) 214–225.
[2] English Heritage, Waterlogged Wood Guidelines on the Recording, Sampling, Conservation and Curation of Waterlogged Wood, English Heritage Publishing, 2010.
[3] M. Bardet, M.F. Foray, Q.-K. Trân, High-resolution solid-state CPMAS NMR study of archaeological woods, Anal. Chem. 74 (6) (2002) 4386–4390.
[4] EN 16873: 2016. Conservation of cultural heritage. Guidelines for the management of waterlogged wood on archaeological terrestrial sites.
[5] D. Capitani, V. Di Tullio, N. Proietti, Nuclear magnetic resonance to characterize and monitor cultural heritage, Prog. Nucl. Mag. Res. Sp. 64 (2012) 29–69.
[6] A. Salanti, L. Zoia, E.L. Tolppa, G. Giachi, M. Orlandi, Characterization of waterlogged wood by NMR and GPC techniques, Microchem. J. 95 (2010) 345–352.
[7] K.E. High, K.E. Penkman, A review of analytical methods for assessing preservation in waterlogged archaeological wood and their application in practice, Herit. Sci. 8 (1) (2020) 1–33.
[8] N. Macchioni, B. Pizzo, C. Capretti, G. Giachi, How an integrated diagnostic approach can help in a correct evaluation of the state of preservation of waterlogged archaeological wooden artefacts, J. Archaeol. Sci. 39 (10) (2012) 3255–3263.
[9] L. Zoia, D. Tamburini, M. Orlandi, J.J. Łucejko, A. Salanti, E.-L. Tolppa, F. Modugno, M.P. Colombini, Chemical characterisation of the whole plant cell wall of archaeological wood: an integrated approach, Anal. Bioanal. Chem. 409 (2017) 4233–4245.
[10] C.G. Björdal, T. Nilsson, G. Daniel, Microbial decay of waterlogged archaeological wood found in Sweden Applicable to archaeology and conservation, Int. Biodeter. Biodegradation 43 (1999) 63–73.
[11] N.B. Pedersen, J.J. Łucejko, F. Modugno, C. Björdal, Correlation between Bacterial Decay and Chemical Changes in Waterlogged Archaeological Wood Analysed by Light Microscopy and Py-GC/MS, Holzforschung, 2020.
[12] R.A. Eaton, M.D. Hale, Wood: Decay, Pests and Protection, Chapman and Hall Ltd, 1993.
[13] R.A. Blanchette, A review of microbial deterioration found in archaeological wood from different environments, Int. Biodeterior. Biodegradation 46 (3) (2000) 189–204.
[14] N.B. Pedersen, C.G. Björdal, P. Jensen, C. Felby, Bacterial degradation of archaeological wood in anoxic waterlogged environments, in: S.E. Harding (Ed.), Stability of Complex Carbohydrate Structures. Biofuel, Foods, Vaccines and Shipwrecks, The Royal Society of Chemistry, Cambridge, 2013, pp. 160–187.
[15] C.G. Björdal, Microbial degradation of waterlogged archaeological wood, J. Cult. Herit. 13 (3) (2012) S118–S122.
[16] Å. Henrik-Klemens, F. Bengtsson, C.G. Björdal, Raman spectroscopic investigation of iron-tannin precipitates in waterlogged archaeological oak, Stud. Conserv. (2021) 1–11.
[17] J.I. Hedges, The chemistry of archaeological wood, in: R.M. Rowell, R.J. Barbour (Eds.), Archaeological Wood - Properties, Chemistry, and Preservation, Advances in Chemistry Series 225, American Chemical Society, Washington DC, 1990, pp. 111–140.
[18] D.J. Cole-Hamilton, B. Kaye, J.A. Chudek, G. Hunter, Nuclear magnetic resonance imaging of waterlogged wood, Stud. Conserv. 40 (1) (1995) 41–50.
[19] E.E. Thybring, M. Kymäläinen, L. Rautkari, Experimental techniques for characterising water in wood covering the range from dry to fully water saturated, Wood Sci. Technol. 52 (2018) 297–329.
[20] R.R. Ernst, G. Bodenhausen, A. Wokaun, Principles of Nuclear Magnetic Resonance in One and Two dimensions, Clarendon Press, Oxford, 1987.
[21] B. Blümich, F. Casanova, J. Perlo, F. Presciutti, C. Anselmi, B. Doherty, Noninvasive testing of art and cultural heritage by mobile NMR, Acc. Chem. Res. 43 (6) (2010) 761–770.
[22] B. Blümich, M. Baias, C. Rehorn, V. Gabrielli, D. Jaschtschuk, C. Harrison, C. Invernizzi, M. Malagodi, Comparison of historical violins by non-destructive MRI depth profiling, Microchem. J. 158 (2020) 105219.
[23] E. Danieli, B. Blümich, Single-sided magnetic resonance profiling in biological and materials science, J. Magn. Reson. 229 (2013) 142–154.
[24] Magritek. http://www.magritek.com/products/nmr-mouse/, 2020 (accessed 20 July 2020).
[25] M.T. Riggin, A.R. Sharp, R. Kaiser, Transverse NMR relaxation of water in wood, J. Appl. Polym. Sci. 23 (1979) 3147–3154.
[26] R.S. Menon, A.L. MacKay, J.R.T. Hailey, M. Bloom, A.E. Burgess, J.S Swanson, An NMR determination of the physiological water distribution in wood during drying, J. Appl. Polym. Sci. 33 (4) (1987) 1141–1155.
[27] D. Topgaard, O. Soderman, Diffusion of water absorbed in cellulose fibers studied with 1H-NMR, Langmuir 17 (2001) 2694–2702.
[28] G. Almeida, S. Gagné, R.E. Hernández, A NMR study of water distribution in hardwoods at several equilibrium moisture contents, Wood Sci. Technol. 41 (4) (2007) 293–307.
[29] P.M. Kekkonen, V.-V. Telkki, J. Jokisaari, Determining the highly anisotropic cell structures of Pinus sylvestris in three orthogonal directions by PGSTE NMR of absorbed water and methane, J. Phys. Chem. B 113 (4) (2009) 1080–1084.
[30] P.M. Kekkonen, V.-V. Telkki, J. Jokisaari, Effect of thermal modification on wood cell structures observed by pulsed-field-gradient stimulated-echo NMR, J. Phys. Chem. C 114 (2010) 18693–18697.
[31] V.-V. Telkki, Wood characterization by NMR & MRI of fluids, eMagRes 1 (2012) 215–222.
[32] E.E. Thybring, L.G. Thygesen, S. Svensson, C.A.S Hill, A critical discussion of the physics of wood–water interactions, Wood Sci. Technol. 47 (2013) 141–161.
[33] C. Terenzi, S.V. Dvinskikh, I. Furó, Wood microstructure explored by anisotropic 1H NMR line broadening: experiments and numerical simulations, Phys. Chem. B 117 (28) (2013) 8620–8632.
[34] V.-V Telkki, M. Yliniemi, J. Jokisaari, Moisture in softwoods: fiber saturation point, hydroxyl site content and the amount of micropores determined from NMR relaxation time distributions, Holzforschung 67 (2013) 291–300.
[35] M. Fredriksson, L. Thygesen, The states of water in Norway spruce (Picea abies (L.) Karst.) studied by low-field nuclear magnetic resonance (LFNMR) relaxometry: assignment of free-water populations based on quantitative wood anatomy, Holzforschung 71 (1) (2017).
[36] K. Xu, J. Lu, Y. Gao, Y. Wu, X. Li, Determination of moisture content and moisture content profiles in wood during drying by low-field nuclear magnetic resonance, Dry. Technol. 35 (15) (2017) 1909–1918.
[37] J. Kowalczuk, A. Rachocki, M. Broda, B. Mazela, G.A. Ormondroyd, J. Tritt-Goc, Conservation process of archaeological waterlogged wood studied by spectroscopy and gradient NMR methods, Wood. Sci. Technol. 53 (2019) 1207–1222.
[38] C. Cai, M. Javed, S. Komulainen, V.-V. Telkki, A. Haapala, H. Heräjärvi, Effect of natural weathering on water absorption and pore size distribution in thermally modified wood determined by nuclear magnetic resonance, Cellulose 27 (2020) 4235–4247.
[39] J. Cox, P.J. McDonald, B.A. Gardiner, A study of water exchange in wood by means of 2D NMR relaxation correlation and exchange, Holzforschung 64 (2010) 259–266.
[40] M. Bonnet, D. Courtier-Murias, P. Faure, S. Rodts, S. Care, NMR determination of sorption isotherms in earlywood and latewood of Douglas fir. Identification of bound water components related to their local environment, Holzforschung 71 (6) (2017) 481–490.
[41] L. Rostom, D. Courtier-Murias, S. Rodts, S. Care, Investigation of the effect of aging on wood hygroscopicity by 2D 1H NMR relaxometry, Holzforschung 74 (4) (2019) 400–411.
[42] S. Hiltunen, A. Mankinen, M.A. Javed, S. Ahola, M. Venäläinen, V.-V. Telkki, Characterization of the Decay Process of Scots Pine Wood Caused by Coniophora Puteana Using NMR and MRI, Holzforschung, 2020.
[43] P.T. Callaghan, Principles of Nuclear Magnetic Resonance Microscopy, Oxford University Press Inc, New York, 1991.
[44] S. Godefroy, P.T. Callaghan, 2D relaxation/diffusion correlations in porous media, Magn. Reson. Imaging 21 (2003) 381–383.
[45] Pedone C. (2019). Restauro del relitto "E" dagli scavi del porto antico di Napoli: due metodi di consolidamento a confronto. Master degree in Conservazione e restauro dei beni culturali, supervisor Antonella Di Giovanni. Istituto superiore per la conservazione ed il restauro, Roma, 244.
[46] Wood anatomy of central European species. http://www.woodanatomy.ch, 2020 (accessed 20 July 2020).

[47] InsideWood. 2004-onwards. http://insidewood.lib.ncsu.edu/search, 2020 (accessed 20 July 2020).
[48] S.E. Anagnost, R.W. Meyer, C. de Zeeuw, Confirmation and significance of Bartholin's method for the identification of the wood of Picea and Larix, IAWA J 15 (2) (1994) 171–184.
[49] D. Giampaola, V. Carsena, G. Boetto, F. Crema, C. Florio, D. Panza, B. Pizzo, C. Capretti, G. Galotta, G. Giachi, N. Macchioni, M.P. Nugari, M. Bartolini, La scoperta del porto di" Neapolis": dalla ricostruzione topografica allo scavo e al recupero dei relitti, Archaeol. Maritima Mediterr. 2 (2005) 1000–1045.
[50] V. Di Donato, M.R. Ruello, V. Liuzza, V. Carsana, D. Giampaola, M.A. Di Vito, C. Morhange, A. Cinque, E.E. Russo, Development and decline of the ancient harbor of Neapolis, Geoarchaeology 33 (2018) 542–557.
[51] M.D. Hürlimann, L. Venkataramanan, Quantitative measurement of two dimensional distribution functions of diffusion and relaxation in grossly inhomogeneous fields, J. Magn. Reson. 157 (2002) 31–42.
[52] M.D. Hürlimann, L. Venkataramanan, C. Flaum, P. Speier, C. Karmonik, R. Freedman, N. Heaton, Diffusion-editing: new NMR measurement of saturation and pore geometry, SPWLA (2002) 2–5.
[53] M.D. Hürlimann, L. Venkataramanan, C. Flaum, The diffusion-spin relaxation time distribution function as an experimental probe to characterize fluid mixtures in porous media, J. Chem. Phys. 117 (22) (2002) 10223–10232.
[54] Y.-Q. Song, L. Venkataramanan, M.D. Hürlimann, M. Flaum, P. Frulla, C. Straley, T1-T2 correlation spectra obtained using a fast two-dimensional Laplace inversion, J. Magn. Reson. 154 (2002) 261–268.
[55] B. Sun, K.J. Dunn, Core analysis with two dimensional NMR, Meteorol. Atmos. Phys. 109 (1) (2002) 61–72.
[56] B. Hills, S. Benamira, N. Marigheto, K. Wright, T1-T2 correlation analysis of complex foods, Appl. Magn. Reson. 26 (2004) 543–560.
[57] B. Sun, K.J. Dunn, A global inversion method for multi-dimensional NMR logging, J. Magn. Reson. 172 (1) (2005) 152–160.
[58] P. Galvosas, P.T. Callaghan, Multi-dimensional inverse Laplace spectroscopy in the NMR of porous media, C. R. Phys. 11 (2010) 172–180.
[59] J. Keeler, Understanding NMR Spectroscopy, John Wiley & Sons Inc, New York, 2010.
[60] D. Bernin, D. Topgaard, NMR diffusion and relaxation correlation methods: new insights in heterogeneous materials, Curr. Opin. Colloid Interface Sci. 18 (2013) 166–172.
[61] Y.-Q. Song, Magnetic resonance of porous media (MRPM): a perspective, J. Magn. Reson. 229 (2013) 12–24.
[62] Y. Zhang, B. Blümich, Spatially resolved D-T2 correlation NMR of Porous Media, J. Magn. Reson. 242 (2014) 41–48.
[63] V.-V. Telkki, Hyperpolarized Laplace NMR, Magn. Reson. Chem. 56 (2018) 619–632.
[64] L. Venkataramanan, Y.-Q. Song, M.D. Hürlimann, Solving Fredholm integrals of the first kind with tensor product structure in 2 and 2.5 dimensions, IEEE Trans. Signal Process. 50 (2002) 1017–1026.
[65] Mailhiot S. (2020). Dataset: Characterization of Waterlogged Archaeological Wood Samples by Single-Sided 1D and 2D NMR. http://urn.fi/urn:nbn:fi:att:c8528ef9-4485-46bd-9175-417481298ed5.
[66] H.G. Richter, D. Grosser, I. Heinz, P.E. Gasson, IAWA List of microscopic features for softwood identification, IAWA J. 25 (2004) 1–70.
[67] S. Capuani, V. Stagno, M. Missori, L. Sadori, S. Longo, High-resolution multiparametric MRI of contemporary and waterlogged archaeological wood, Magn. Reson. Chem. 58 (9) (2020) 860–869.
[68] P.O. Kettunen, Wood Structure and Properties, Trans Tech Publications, Ltd, 2006.
[69] E.A. Wheeler, P. Baas, P.E. Gasson, IAWA List of microscopic features for hardwood identification, IAWA Bull. 10 (3) (2007) 219–332 n. s..
[70] M. Baias, B. Blümich, Nondestructive testing of objects from cultural heritage with NMR, in: G. Webb (Ed.), Modern Magnetic Resonance, Springer, Cham, 2018.
[71] C. Casieri, F. De Luca, P. Fantazzini, Pore-size evaluation by single-sided nuclear magnetic resonance measurements: compensation of water self-diffusion effect on transverse relaxation, J. Appl. Phys. 97 (4) (2005) 043901.
[72] S. De Santis, M. Rebuzzi, G. Di Pietro, F. Fasano, B. Maraviglia, S. Capuani, In vitro and in vivo MR evaluation of internal gradient to assess trabecular bone density, Phys. Med. Biol. 55 (2010) 5767.
[73] H.Y. Carr, E.M. Purcell, Effects of diffusion on free precession in nuclear magnetic resonance experiments, Phys. Rev. 94 (1954) 630–638.
[74] V.-V Telkki, V.V. Zhivonitko, Ultrafast NMR diffusion and relaxation studies, Annu. Rep. NMR Spectrosc. 97 (2019) 83–119.
[75] W. Wycoff, S. Pickup, B. Cutter, W. Miller, T.C. Wong, The determination of the cell size in wood by nuclear magnetic resonance diffusion techniques, Wood Fiber Sci. 32 (2000) 72–80.
[76] M. Urbanczyk, Y. Kharbanda, O. Mankinen, V.-V. Telkki, Accelerating restricted diffusion NMR studies with time-resolved and ultrafast methods, Anal. Chem. 92 (2020) 9948–9955.
[77] S. Longo, S. Capuani, C. Corsaro, E. Fazio, Silver fir characterized by micro-imaging NMR and FTIR spectroscopy, IOP Conf. Ser. Mater. Sci. Eng. 777 (2020) 012004.